Pharmaceutical Cocrystals of Niclosamide

ARTICLE *in* CRYSTAL GROWTH & DESIGN · JULY 2012

Impact Factor: 4.89 · DOI: 10.1021/cg300784v

3 AUTHORS:

Palash Sanphui
Indian Institute of Science
26 PUBLICATIONS **512** CITATIONS

SEE PROFILE

Dr Sudalai Kumar S
The Francis Xavier Engineering College
32 PUBLICATIONS **57** CITATIONS

SEE PROFILE

Ashwini Nangia
University of Hyderabad
273 PUBLICATIONS **7,113** CITATIONS

SEE PROFILE

CRYSTAL GROWTH & DESIGN

Article

pubs.acs.org/crystal

Pharmaceutical Cocrystals of Niclosamide

Palash Sanphui, S. Sudalai Kumar, and Ashwini Nangia*

School of Chemistry, University of Hyderabad, Prof. C. R. Rao Road, Central University P.O., Gachibowli, Hyderabad 500 046, India

Supporting Information

ABSTRACT: Niclosamide (NCL) is an anthelmintic BCS class II drug of low solubility and high permeability. Pharmaceutical cocrystals of NCL were prepared with GRAS molecules, such as caffeine (CAF), urea (URE), *p*-aminobenzoic acid (PABA), theophylline (THPH), nicotinamide (NCT), and isonicotinamide (INA), to improve drug solubility. Neat grinding, wet granulation, and slow evaporation methods were successful to make niclosamide cocrystals. All new crystalline forms were characterized by X-ray diffraction, differential scanning calorimetry, and IR-Raman spectroscopy to confirm their purity and homogeneity. X-ray crystal structures provided details of hydrogen bonding, molecular packing, and drug···coformer interactions. The intermolecular O−H···O hydrogen bond from the hydroxyl donor to the carbonyl acceptor in the niclosamide crystal structure was replaced by an acceptor atom of the coformer in cocrystal structures. Cocrystals with nicotinamide and isonicotinamide were characterized by ^{13}C ss-NMR spectroscopy because their single crystals could not be obtained. All cocrystals, except NCL−PABA, showed a faster powder dissolution rate than the reference active pharmaceutical ingredient (API). Niclosamide−theophylline acetonitrile solvate showed the highest solubility (6 times compared to the API) among all the crystalline forms. NCL−THPH cocrystals showed comparably good dissolution (5 times faster than the drug) up to 90 min. The solubility advantage of the cocrystal was diminished by transformation to insoluble niclosamide monohydrate within 1 h of the dissolution experiment in 40% i-PrOH−water. Equilibrium solubility experiments showed that all cocrystals as well as the pure API transformed to NCL monohydrate within 24 h in 40% i-PrOH−water slurry medium. Among the cocrystals studied, NCL−NCT and NCL−INA exhibited better stability under accelerated humidity conditions (75% RH, 40 °C), but they did not have the same solubility advantage as the fast dissolving species NCL−THPH.

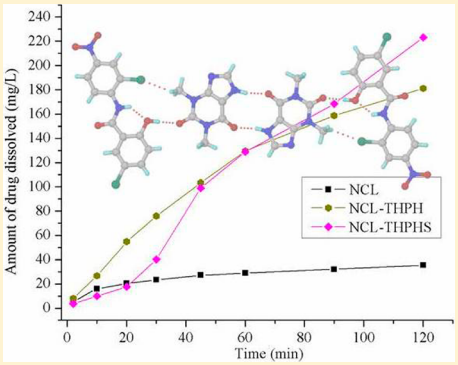

INTRODUCTION

Approximately 40% of drugs in the marketplace and 70% of new chemical entities in the discovery pipeline are poorly water-soluble. An improvement in the solubility of oral drugs can enhance their bioavailability and therapeutic potential. Identifying the optimum solid form of an active pharmaceutical ingredient (API) is a challenge in clinical development, a stage in the drug discovery chain that has assumed an even greater significance in the current decade of fewer new chemical entities being launched.[1] Most APIs are crystalline solids at room temperature and are commonly delivered as a solid oral dosage form (such tablet, capsule, etc.). It is well established that different solid forms (e.g., polymorphs, hydrates, solvates, amorphous, salts, and cocrystals) of the same compound have different physicochemical properties such as solubility, bioavailability, stability, tableting, etc.[2] Cocrystals consist of two or more solid components (at ambient conditions) in a definite stoichiometric ratio held together by noncovalent interactions, for example, hydrogen bonds. A pharmaceutical cocrystal[3] is a multicomponent solid form of an API with a GRAS (Generally Regarded As Safe)[4] partner molecule. Since pharmaceutical cocrystals are molecular complexes held together by hydrogen bonds, the API is not modified covalently and hence the active drug species at the site of biological action is the same. Second, if the coformer has high solubility then the drug cocrystal will often dissolve faster than the API. Cocrystals can offer the dual advantage of high solubility and good stability of the API in the same solid phase.[3a,c,i,j] The analysis of dissolution kinetics for a series of cocrystals with the reference API will provide a better understanding on the role of hydrogen bonding and coformer nature on drug dissolution and solubility.[3a−d,k]

Niclosamide[5] (chemical name 2,5-dichloro-4-nitrosalicylanilide, Figure 1, NCL hereafter) is an anthelmintic drug used for the treatment of worm infestations in humans and animals. It inhibits the replication of several acute respiratory syndrome coronavirus.[6] NCL is available in two dosage forms, tablets and suspensions. It is a BCS Class II drug marketed as Niclocide tablet (500 mg dose, dose number Do = 200). Niclosamide is among the essential orally administered drugs with inclusive data.[7] It is practically insoluble in water, sparingly soluble in organic solvents such as diethyl ether, THF, ethyl acetate, dioxane, etc. and is usually formulated as a suspension. The liquid dosage form contains an appropriate quantity of the drug mixed in a small volume. Both niclosamide anhydrate and niclosamide monohydrate are available for drug formulation.[8]

Received: June 9, 2012
Revised: July 18, 2012
Published: July 24, 2012

dx.doi.org/10.1021/cg300784v | *Cryst. Growth Des.* 2012, 12, 4588−4599

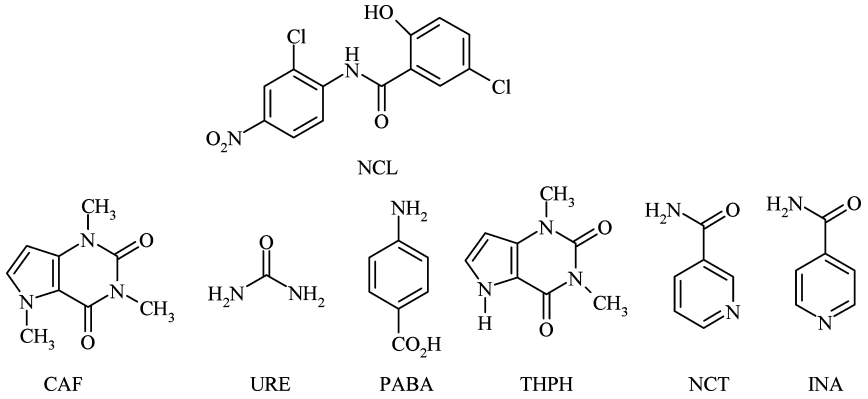

Figure 1. Chemical structure of niclosamide (NCL) and coformers caffeine (CAF), urea (URE), *p*-aminobenzoic acid (PABA), theophylline (THPH), nicotinamide (NCT), and isonicotinamide (INA). All niclosamide cocrystals are of 1:1 stoichiometry.

However, given the high affinity of niclosamide anhydrate for water, various suspension formulations transform to cement-like sediments of the hydrate during storage.[9] Two monohydrates, an anhydrate, and a few solvates of niclosamide are reported in the literature.[5b] Photolysis of niclosamide in pH 5 buffer is 4.3 times faster than pH 9 buffer and 1.5 times faster than in pH 7 buffer medium.[10] Niclosamide has a high tendency to make solvates, similar to the drug axitinib.[11] The aqueous solubility of niclosamide is 13−15 mg/L and the solubility order is anhydrous ≫ solvates > hydrates.[5c]

The pharmaceuticals cocrystals approach was attempted to modify the solubility of Niclosamide and prevent transformation to hydrate, because the latter product has even lower solubility (0.45−0.55 mg/L). Niclosamide hydration is similar to caffeine and nitrofurantoin hydrate transformation.[12] Anhydrous white niclosamide transforms to greenish monohydrate within one month of storage at ambient conditions. Hydrates are generally not preferred for clinical purpose because of lower solubility and variable drug activity with water composition in the hydrate. NCL−phosphate and NCL−ethanolamine salts of higher solubility are reported in recent patents.[13] However, hydration is a common byproduct of salts and in this respect cocrystals are preferred even though they provide only modest solubility advantage (4−20 times) compared to salts (500−1000 times).[14] Moreover, the neutral functional groups in niclosamide molecule (amide, phenol) preclude salt formation and pharmaceutical cocrystallization is a promising alternative to improve solubility and dissolution rate. There are no niclosamide cocrystals reported in the literature to improve API pharmacokinetics. Pharmaceutical cocrystals of niclosamide with GRAS molecules (caffeine, urea, *p*-aminobenzoic acid, theophylline, nicotinamide, and isonicotinamide; see Figure 1) were prepared by solvent drop grinding and characterized using IR-Raman spectroscopy, thermal differential scanning calorimetry (DSC) and thermogravimetric analysis (TGA), single crystal and powder X-ray diffraction (PXRD), and solid-state NMR spectroscopy.

RESULTS AND DISCUSSION

Niclosamide has a strong tendency to form solvates when crystallized from solution. Anhydrous niclosamide, monohydrates H_A and H_B, and THF, tetraethylene glycol, DMF, DMSO, MeOH solvates of niclosamide were characterized by PXRD, DSC, and FT-IR. Crystal structures of the monohydrate, tetrahydrofuran and tetraethylene glycol solvates are known.[5a] However, no guest-free X-ray single crystal structure of the API is reported. Solvent-free crystallization by melting and sublimation[15] afforded a guest-free structure of niclosamide. Niclosamide cocrystals (1:1) were obtained from dry EtOAc and CH_3CN solvents after grinding the components in mortar-pestle. Dry solvents were necessary in cocrystallization; otherwise hydrate formation was a side product. Wet granulation[16] enhances reaction kinetics to give improved yields of cocrystals. The formation of new solid-state forms was established by FT-IR, melting point, and PXRD. Crystallographic parameters for niclosamide and its novel cocrystals are summarized in Table 1, and ORTEP diagrams are displayed in Figure S1, Supporting Information.

CRYSTAL STRUCTURE ANALYSIS

Niclosamide (NCL). Niclosamide crystallized in the monoclinic space group $P2_1/c$ with one molecule in the asymmetric unit. The molecule is locked in a near planar conformation through intramolecular N−H···O hydrogen bond (1.76 Å, 142°). Intermolecular O−H···O hydrogen bond (1.72 Å, 173°) from hydroxyl to carbonyl group extends in a chain along the *c*-axis (Figure 2a). Hydrogen bonds were normalized using Platon (Table 2). Niclosamide molecules are connected by Cl···NO_2 interaction (3.22 Å) in a dimer motif of graph set notation[17] $R_2^2(12)$ ring. $\pi-\pi$ stacking of layers (at 3.34 and 3.39 Å separation) along the *b*-axis (Figure 2b) completes the structure description. The crystal structure of guest-free niclosamide is different from its monohydrates[5a] where water molecules are present in the cavity formed by niclosamide molecules, which stabilize the hydrate structure through two water to niclosamide O−H···O hydrogen bonds.

Niclosamide−Caffeine (NCL−CAF, 1:1). The crystal structure of NCL−CAF (1:1) cocrystal was solved in monoclinic space group $P2_1/c$. The intramolecular N−H···O hydrogen bond (1.76 Å, 143°) of niclosamide persists in the cocrystal structure. Two niclosamide molecules form C−H···O dimer (2.26 Å, 141°) of $R_2^2(12)$ ring motif (Figure 3a). There is a strong O−H···O bond between the components (1.66 Å, 173°) from O−H of niclosamide to the carbonyl acceptor of caffeine. The molecules are arranged in ABBA fashion along the *a*-axis through $\pi-\pi$ stacking (3.32 Å) (Figure 3b).

Niclosamide−Urea (NCL−URE, 1:1). The asymmetric unit in space group $P2_1/c$ contains one molecule each of niclosamide and urea. Intramolecular N−H···O hydrogen bond (1.79 Å, 139°) in niclosamide makes available the OH donor for the O−H···O hydrogen bond (1.62 Å, 176°) with urea in an orthogonal orientation (angle between molecular

dx.doi.org/10.1021/cg300784v | *Cryst. Growth Des.* 2012, 12, 4588−4599

Table 1. Crystallographic Parameters for Niclosamide and Its Cocrystals

	NCL	NCL−CAF	NCL−URE	NCL−PABA	NCL−THPH	NCL−THPHS
emp formula	$C_{13}H_8N_2O_4Cl_2$	$C_{13}H_8N_2O_4Cl_2{\cdot}C_8H_{10}N_4O_2$	$C_{13}H_8N_2O_4Cl_2{\cdot}CH_4N_2O$	$C_{13}H_{12}N_2O_4Cl_2{\cdot}C_7H_7NO_2$	$C_{13}H_8N_2O_4Cl_2{\cdot}C_7H_8N_4$	$C_{13}H_8N_2O_4Cl_2{\cdot}C_7H_8N_4{\cdot}C_2H_3N$
formula wt	327.11	521.31	387.18	464.25	507.29	548.34
crystal system	monoclinic	monoclinic	monoclinic	triclinic	monoclinic	triclinic
space group	$P2_1/c$	$P2_1/c$	$P2_1/c$	$P\bar{1}$	$P2_1/c$	$P\bar{1}$
T (K)	100	100	100	298	298	100
a (Å)	13.485(2)	7.8756(4)	11.1272(10)	7.2810(14)	9.1371(7)	8.579(3)
b (Å)	7.0669(11)	10.7632(6)	16.9312(14)	12.763(2)	10.8809(9)	10.733(4)
c (Å)	13.510(2)	25.8869(13)	8.5708(7)	12.789(2)	22.4497(17)	13.216(5)
α (°)	90	90	90	62.543(17)	90	105.579(6)
β (°)	98.345(2)	96.286(1)	93.312(1)	76.384(16)	99.924(8)	94.104(6)
γ (°)	90	90	90	74.384(15)	90	96.024(6)
volume (Å^3)	1273.9(3)	2181.2(2)	1612.0(2)	1007.0(3)	2198.6(3)	1159.4(7)
D_{calcd}/g cm^{-3}	1.706	1.588	1.595	1.531	1.533	1.571
μ/mm^{-1}	0.527	0.352	0.438	0.367	0.347	0.337
Z	4	4	4	2	4	2
range h	−16 to +16	−9 to +9	−13 to +13	−9 to +9	−11 to +11	−10 to +10
range k	−8 to +8	−13 to +13	−20 to +20	−15 to +15	−13 to +13	−13 to +13
range l	−16 to +16	−31 to +31	−10 to +10	−15 to +15	−28 to +28	−16 to +16
reflns collected	12392	22138	16535	8234	10097	8740
unique reflns	2490	4300	3196	4098	4499	4527
observed reflns	2326	4010	3001	2225	2389	3908
R_{int}, R_1 ($I > 2\sigma(I)$)	0.0411, 0.0349	0.0289, 0.0547	0.0319, 0.0313	0.0299, 0.0386	0.0510, 0.0614	0.0532, 0.0526
$wR(F^2)$ ($I > 2\sigma(I)$), $wR(F^2)$ (all data)	0.915, 0.0931	0.1531, 0.1555	0.0766, 0.0782	0.0763, 0.0861	0.1032, 0.1358	0.1394, 0.1728
$\Delta\rho_{max}$, $\Delta\rho_{min}$/Å^{-3} (largest peak, hole elec density)	0.405, −0.401	1.930, −0.649	0.326, −0.268	0.156, −0.199	0.233, −0.342	0.494, −0.732
GOF	1.093	1.039	1.069	0.857	0.998	1.03
diffractometer	Bruker SMART	Bruker SMART	Bruker SMART	Oxford Gemini	Oxford Gemini	Bruker SMART

dx.doi.org/10.1021/cg300784v | Cryst. Growth Des. 2012, 12, 4588−4599

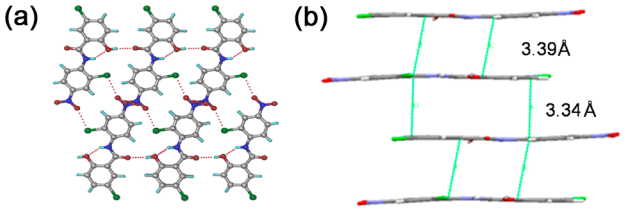

Figure 2. (a) O−H···O interaction between niclosamide molecules results in a layered structure along the *c*-axis in niclosamide. (b) Niclosamide molecules form $\pi-\pi$ stacking interaction between the layers parallel to the *b*-axis.

planes 83.8°). The urea α-tape motif[18] along the *c*-axis (N−H···O: 09 Å, 145°; 1.98 Å, 152°) is bonded to amide C═O through the N−H···O hydrogen bond (1.99 Å, 152°). Two niclosamide and two urea molecules form a cyclic $R_6^4(20)$ ring motif (Figure 4a). Urea and niclosamide molecules are arranged in an ABAB fashion such that $\pi-\pi$ stacking of niclosamide (3.34 Å) and the α-network translation of urea (N···N 4.38 Å) are about roughly matched in distance separation (Figure 4b), due to slight up−down tilt of urea molecules in the linear array.

Niclosamide−PABA (NCL−PABA, 1:1). NCL−PABA (1:1) cocrystal ($P\bar{1}$) contains a COOH dimer of PABA in $R_2^2(8)$ ring motif (H···O: 1.63 Å, 179°) hydrogen bonded to niclosamide through NH···O_2N and CH···O_2N hydrogen bonds (2.19 Å, 154°; 2.58 Å, 154°) along the *c*-axis (Figure 5a). Two niclosamide and two PABA molecules form a tetramer of $R_6^4(16)$ ring motif through both N−H···O and O−H···N hydrogen bonds (2.02 Å, 157°; 1.82 Å, 173°) parallel to the (200) plane (Figure 5b). Niclosamide molecules connect to the next layer by $\pi-\pi$ stacking (3.38 Å).

Niclosamide−Theophylline (NCL−THPH, 1:1). NCL−THPH (1:1) was crystallized from i-PrOAc and the crystal structure was solved in the monoclinic space group $P2_1/c$. The API and theophylline form intermolecular hydrogen bond (H···O: 1.69 Å, 179°) from the hydroxyl donor of the drug to the carbonyl acceptor of theophylline. Theophylline molecules form a centrosymmetric carboxamide dimer of $R_2^2(10)$ ring through the N−H···O bond (1.84 Å, 168°) (Figure 6a). There is a weak C−H···O interaction (2.24 Å, 142°) between inversion-related niclosamide molecules. These tetramer units are connected to the next layer by an auxiliary C−H···O interaction (2.56 Å, 144°) from theophylline aromatic ring C−H to O_2N acceptor of niclosamide along the *c*-axis in a sheet structure (Figure 6b). Two niclosamide and two theophylline molecules are arranged in an ABBA fashion.

Niclosamide−Theophylline Acetonitrile Solvate (NCL−THPHS−CH_3CN, 1:1:1). Niclosamide−theophylline CH_3CN solvate (abbreviated NCL−THPHS) was crystallized from EtOAc−CH_3CN mixture (1:1) and its crystal structures solved in triclinic space group $P\bar{1}$. An intermolecular O−H···O hydrogen bond (1.66 Å, 174°) between the API and theophylline connects the molecules. Two theophylline molecules form centrosymmetric carboxamide dimer through the N−H···O hydrogen bond (1.75 Å, 175°) of $R_2^2(10)$ ring motif (Figure 7a). Acetonitrile solvent molecules are present in channels down the *c*-axis (Figure 7b), similar to niclosamide THF solvate.[5a] A characteristic feature of the crystal is desolvation of acetonitrile from the crystal lattice within 1 h and loss of crystallinity at ∼80 °C (discussed later).

Powder X-ray Diffraction. Niclosamide was purchased as an anhydrous powder from Sigma-Aldrich (Hyderabad, India) and used without further purification. Storage at ambient conditions of 30−40 °C and 50−75% relative humidity (Hyderabad climate) gave a greenish material of niclosamide monohydrate within one month. The transformation was monitored by PXRD and color change. Niclosamide hydrate reverted back to the anhydrous form by heating at 100 °C for 5−6 h. PXRD[19] is a diagnostic tool to differentiate between cocrystals, anhydrate, hydrate, and solvate forms of drugs at a precision of typically $\Delta 2\theta > \pm 0.2°$. The PXRD pattern of niclosamide cocrystals (discussed earlier) matched with the calculated lines from the crystal structure, confirming the purity and homogeneity of the bulk phases (Figure S2). Niclosamide−nicotinamide (NCL−NCT, 1:1) and niclosamide−isonicotinamide (NCL−INA, 1:1) cocrystals were obtained from dry CH_3CN by solvent-assisted grinding for 15 min. However, diffraction quality single crystals could not be obtained by crystallization from different solvents. The cocrystal stoichiometry was ascertained as 1:1 API/coformer based on mixing ratio and ^{1}H NMR of the crystal in DMSO-d_6. The product solids were ascertained as new phases by PXRD. There are noticeable differences in the peak positions of NCL−NCT and NCL−INA cocrystals compared to the pure API and coformer diffraction lines (Figure 8). Two types of niclosamide monohydrates (H_A and H_B) are known in the literature.[5b] PXRD of niclosamide monohydrate H_A (no 3D coordinates reported in the CSD) exhibited characteristic reflections at 2θ 9.47, 11.40, 16.83, 22.43, and 25.54 ± 0.2°. Monohydrate H_B (CSD refcode OBEQER)[5a] exhibited characteristic lines at 2θ 10.37, 13.07, 17.63, 19.02, and 21.0 ± 0.2°.

Thermal Stability of Niclosamide Cocrystals. The thermal stability and phase transition of drugs are important to study physicochemical and pharmacokinetic properties. DSC indicated that NCL−THPH and NCL−NCT showed a second endotherm before melting, perhaps due to phase transition or decomposition. Evolution of CH_3CN from NCL−THPHS solvate occurred at 82 °C and the second endotherm for melting point of the desolvated cocrystal was observed at 209 °C. DSC of niclosamide and its remaining cocrystals exhibited single endotherm peaks confirming thermal stability of the new solid phases (Figure 9). Melting points are listed in Table 3. TGA supports the exact equimolar stoichiometry of niclosamide−theophylline CH_3CN solvate (calc. 7.32%, obsd. 7.48%, Figure S3). The single endotherm in NCL−CAF, NCL−URE, and NCL−INA cocrystals suggested no decomposition prior to melting. The melting point of cocrystals is in between that of the API and the coformer.

IR and Raman Spectroscopy. Infrared and Raman spectroscopy[20] are quantitative tools for the characterization and identification of different solid-state forms. These spectra are based on the vibrational modes of a compound and are extremely sensitive to the structure, hydrogen bonding, molecular conformations, and environment of the API. In general phenolic OH absorbs strongly in the stretching region of 3700−3584 cm^{-1}. According to Moffat et al.,[20d] principal peaks of niclosamide analyzed in KBr disk appear at 1572 (N−H bend), 1515 (NO_2 asymmetric), 1613 (C═C), 1650 (C═O), and 1218 (C−O) cm^{-1}. In the IR spectra (KBr disk) of niclosamide anhydrate and cocrystals, some of the bands were shifted relative to that in the pure API and coformer (Table 4). A change in both carbonyl and amide IR stretching frequencies indicated the formation of a new cocrystal phase. OH stretching

dx.doi.org/10.1021/cg300784v | *Cryst. Growth Des.* 2012, 12, 4588−4599

Table 2. Hydrogen Bonds in Crystal Structures (Neutron-Normalized Distance)

	interaction	d(H···A) (Å)	d(D···A) (Å)	∠D−H···A (deg)	symmetry code
NCL	N1−H1···Cl1	2.36	2.902(2)	113	intramolecular
	N1−H1···O4	1.76	2.630(2)	142	intramolecular
	O4−H2···O3	1.72	2.693(2)	172	$x, 1/2 - y, -1/2 + z$
	C3−H3···O2	2.50	3.363(2)	136	$1 - x, 1 - y, -z$
	C5−H5···Cl2	2.70	3.777(2)	176	$-x, 1/2 + y, 1/2- z$
	C6−H6···O3	2.23	2.896(2)	117	intramolecular
NCL−CAF (1:1)	N1−H1···Cl1	2.42	2.918(2)	109	intramolecular
	N1−H1···O4	1.76	2.640(3)	142	intramolecular
	O4−H2···O5	1.66	2.640(3)	176	$1 - x, 1 - y, 1 - z$
	C5−H5···O3	2.27	3.183(3)	141	$-x, 2 - y, -z$
	C6−H6···O3	2.21	2.876(3)	117	intramolecular
	C11−H11··O9	2.26	3.304(3)	161	$1 - x, -y, -z$
	C14−H14B··O9	2.24	2.732(4)	105	intramolecular
	C16−H16A··O5	2.32	2.779(4)	103	intramolecular
	C16−H16A··Cl1	2.79	3.275(2)	107	$1 - x, 1 - y, 1 - z$
	C20−H20B··O1	2.39	3.387(4)	152	$-x, -3/2 + y, 1/2 - z$
NCL−URE (1:1)	N1−H1···Cl1	2.45	2.959(1)	111	intramolecular
	N1−H1···O4	1.80	2.644(1)	139	intramolecular
	O4−H2···O5	1.62	2.600(1)	176	$1 - x, -y, -z$
	N3−H3A···Cl2	3.07	3.630(1)	116	$-1 + x, 1/2 - y, 1/2+z$
	N3−H3A···O5	2.09	2.974(1)	145	$x, 1/2 - y, 1/2 + z$
	N3−H3B···Cl2	2.58	3.530(1)	157	$-1 + x, y, z$
	N3−H3B···O2	2.56	3.279(1)	128	$-x, 1/2 + y, 1/2 - z$
	N4−H4A···O3	1.99	2.921(1)	152	x, y, z
	N4−H4B···O5	1.98	2.918(1)	152	$x, 1/2 - y, 1/2 + z$
	C3−H3···Cl2	2.69	3.751(1)	168	$1 - x, -1/2+ y, 1/2 - z$
	C6−H6···O3	2.12	2.813(1)	119	intramolecular
	C11−H11···O1	2.24	3.238(1)	153	$1 + x, y, -1 + z$
	C12−H12···O5	2.63	3.365(1)	124	$1 - x, -y, -z$
NCL−PABA (1:1)	N1−H1···Cl1	2.42	2.936(2)	111	intramolecular
	N1−H1···O4	1.82	2.668(2)	139	intramolecular
	O4−H2···N3	1.82	2.803(3)	173	x, y, z
	N3−H3A···O3	2.03	2.981(3)	157	$1 - x, -y, 1 - z$
	N3−H3B···O1	2.19	3.132(3)	155	$x, -1 + y, 1 + z$
	C6−H6···O3	2.14	2.827(3)	119	intramolecular
	C11−H11···O6	2.39	3.401(3)	156	$x, -1 + y, z$
	N1−H1···Cl1	2.35	2.927(3)	115	intramolecular
NCL−THPH (1:1)	N1−H1···O4	1.85	2.654(4)	135	intramolecular
	O4−H2···O6	1.69	2.676(4)	179	$2 - x, 1 - y, -z$
	N5−H5A···O5	1.84	2.835(5)	168	$-x, 2 - y, -z$
	C5−H5···O3	2.24	3.165(5)	142	$1 - x, 1 - y, -z$
	C16−H16···O1	2.50	3.436(5)	144	$x, 3/2 - y, 1/2 + z$
	C6−H6···O3	2.11	2.807(4)	119	intramolecular
	C19−H19A···O2	2.51	3.246(4)	124	$1 - x, 1/2 + y, -1/2 - z$
	C19−H19B···O5	2.27	2.740(4)	104	intramolecular
	C20−H20B···N6	2.46	2.942(5)	105	intramolecular
NCL−THPHS (1:1:1)	O4−H2···O5	1.65	2.629(3)	174	$1 + x, y, z$
	N5−H5A···O6	1.74	2.749(3)	174	$1 - x, 1 - y, 1 - z$
	N1−H1···Cl1	2.47	2.927(3)	107	intramolecular
	N1−H1···O4	1.79	2.650(2)	141	intramolecular
	C2−H2···O4	2.24	3.149(3)	140	$1 - x, 1 - y, 2 - z$
	C10−H10···O2	2.35	3.150(3)	129	$2 - x, 1 - y, 1 - z$
	C11−H11···O4	2.14	2.811(3)	117	intramolecular
	C12−H12···N3	2.37	3.429(3)	163	$1 + x, y, z$
	C21−H21A···Cl2	2.71	3.628(3)	142	$1 - x, -y, 1 - z$
	C21−H21B···O6	2.47	3.542(3)	170	$1 - x, 1 - y, 2 - z$

frequencies at 3490 and 3577 cm^{-1} are characteristic of niclosamide hydrate. Similarly Raman spectra differences in carbonyl, amide as well as nitro stretching frequencies were noted (Table 5). Though single crystals were not possible for NCL−NCT and NCL−INA, changes in IR (Figure S4) and Raman frequencies clearly suggested new solid phases.

dx.doi.org/10.1021/cg300784v | *Cryst. Growth Des.* 2012, 12, 4588−4599

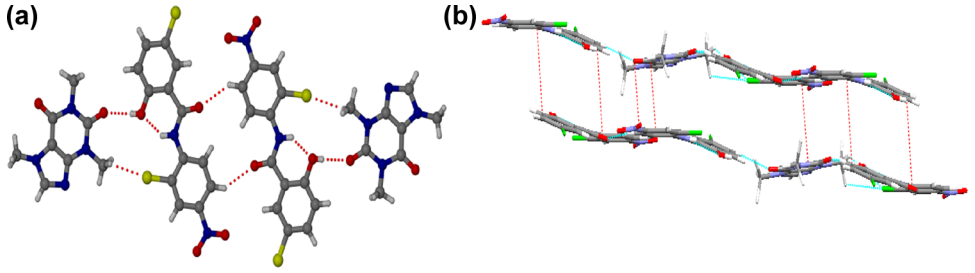

Figure 3. (a) NCL−CAF (1:1) cocrystal forms O−H···O and C−H···O hydrogen bond in a 1D chain. (b) $\pi - \pi$ stacking interaction (3.37 Å) between the aromatic rings of niclosamide and also with caffeine in two successive layers along the *a*-axis.

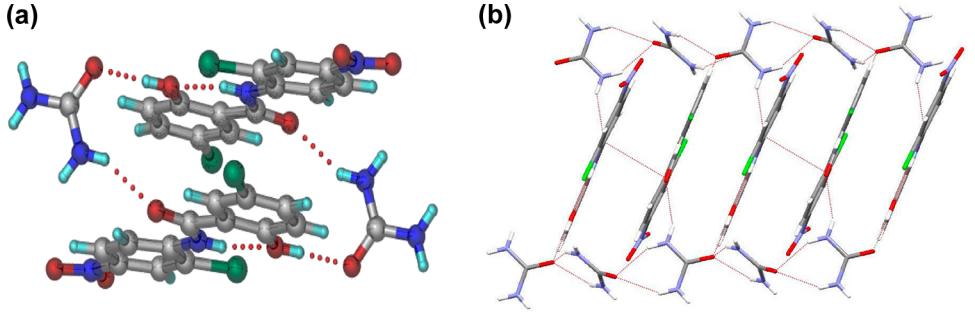

Figure 4. (a) Niclosamide and urea molecules form cyclic $R_6^4(20)$ ring motif between carbonyl oxygen of niclosamide molecule and urea N−H. (b) Two antiparallel urea tape form a column in which niclosamide molecules are stacked through $\pi-\pi$ interactions at 3.34 Å.

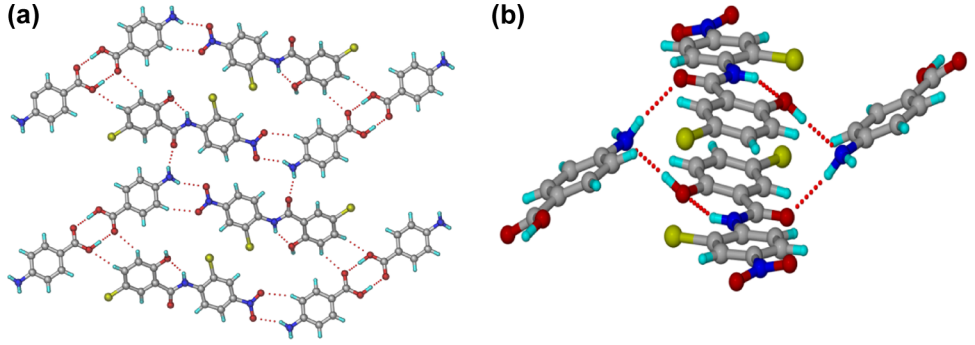

Figure 5. (a) NCL−PABA cocrystals interact through $NH_2\cdots NO_2$ hydrogen bond along the *c*-axis. (b) Two niclosamide and two PABA molecules form $R_6^4(16)$ ring through N−H···O and O−H···N hydrogen bond.

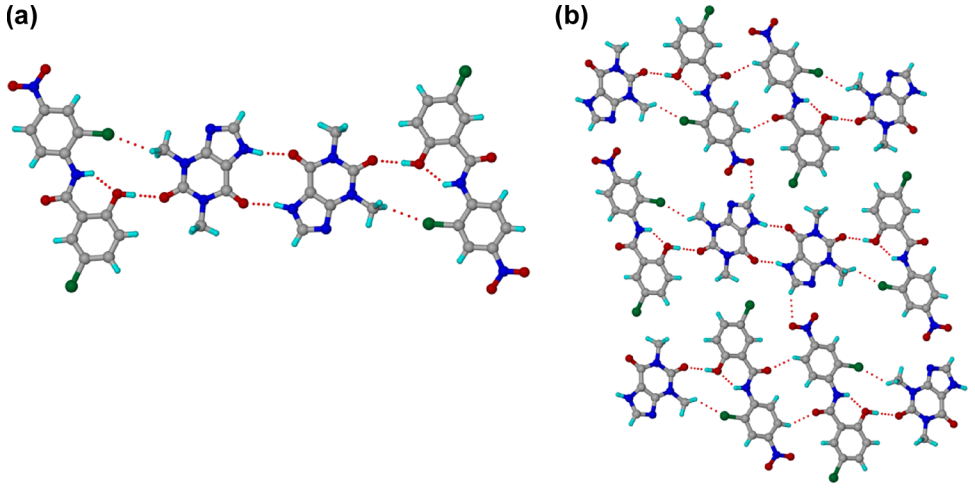

Figure 6. (a) Niclosamide and theophylline molecules arrange as ABBA fashion interacting through O−H···O and N−H···O hydrogen bonds in NCL−THPH cocrystals. (b) Tetramer motif consists of two niclosamide and two theophylline molecules further interacted through C−H···O interaction between niclosamide and theophylline along the *c*-axis completing the overall packing.

dx.doi.org/10.1021/cg300784v | *Cryst. Growth Des.* 2012, 12, 4588−4599

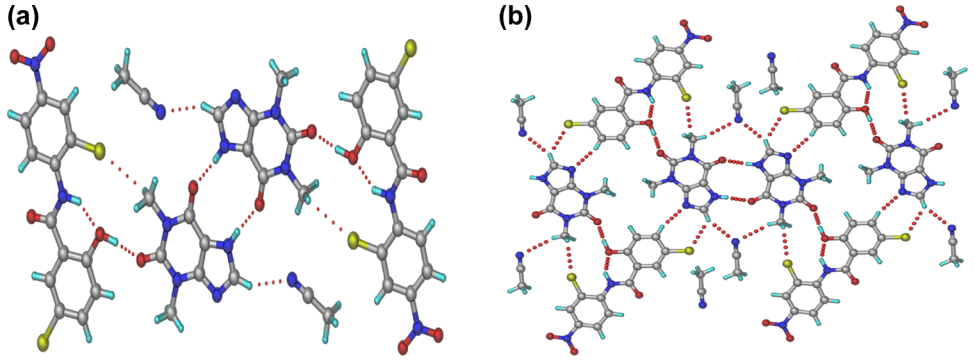

Figure 7. (a) Theophylline carboxamide dimer followed by intermolecular hydrogen bond between niclosamide and theophylline as NCL−THPH cocrystal. (b) Acetonitrile resides in the channel created by niclosamide and theophylline molecules down the *a*-axis.

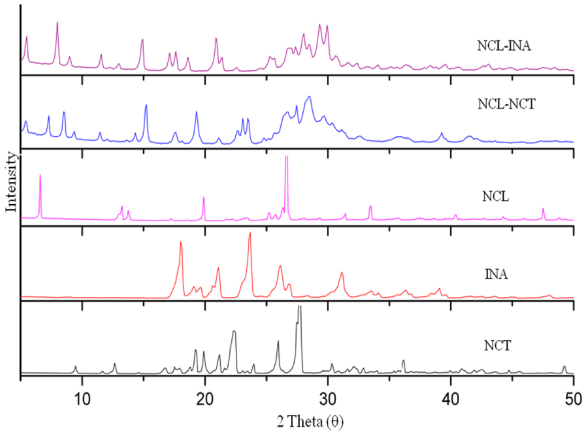

Figure 8. PXRD peaks of NCL−NCT and NCL−INA cocrystal with that of niclosamide and the coformer confirm a new solid phase.

Solid-State NMR Spectroscopy. Solid-state ^{13}C NMR spectroscopy[21] provides structural information on differences in hydrogen bonding, molecular conformations, molecular mobility, and short-range interactions. To confirm the purity as well as stoichiometry of cocrystals, solution ^{1}H NMR spectra were recorded in DMSO-d_6 for NCL−NCT and NCL−INA and further characterized by ^{13}C ss-NMR spectroscopy (Figure 10). Analysis of chemical shifts (in ppm) for NCL−NCT and NCL−INA cocrystals along with that for the API and coformer (Table S1) showed that the carbonyl peak of niclosamide is deshielded from 161.7 to 163.1 ppm and that for nicotinamide moves upfield from 168.9 to 167.7 ppm (corresponding shifts in NCL−INA are 161.8, 164.9, and 168.3 ppm), clear indication for new cocrystals. The absence of an abrupt change in chemical shift (5−10 ppm) for carbonyl peak and also large pK_a differences rule out salt formation. Both solution and ss-NMR spectra indicate 1:1 stoichiometry for NCL−NCT and NCL−INA.

Physical Form Stability. One of the most important characteristics to be determined for any solid drug form is how stable it is to changes in relative humidity and temperature so that it can be stored without affecting drug activity. Pharmaceutical cocrystals, for example, indomethacin−saccharin, ibuprofen−nicotinamide, flurbiprofen−nicotinamide,[3i,22] are shown to be less hygroscopic than the pure APIs. Anhydrous niclosamide at 37 °C and 75% RH converted to monohydrate within 2 weeks.[5b] In contrast niclosamide cocrystals were stable at accelerated ICH conditions[23] of 40 °C and 75% RH for up to 7 weeks as judged by PXRD. NCL−PABA, NCL−URE, and NCL−CAF cocrystals were stable for 2, 4, and 6 weeks respectively (Figure 11). The reference drug NCL and NCL−THPHS converted to niclosamide monohydrate within 1 week (Figure S5, Supporting Information).

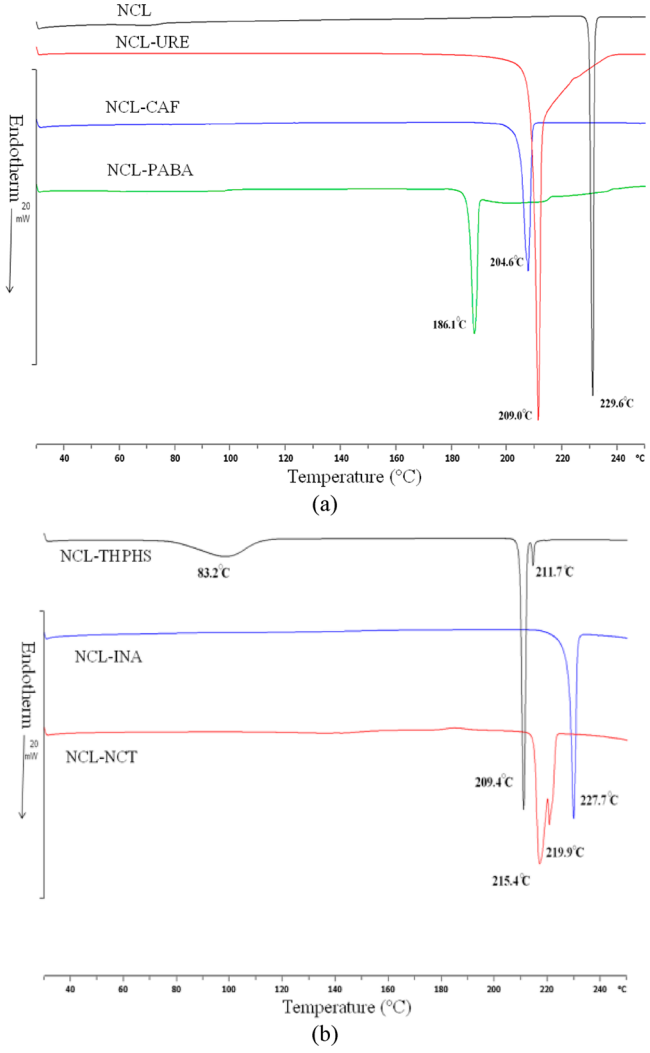

Figure 9. (a, b) DSC endotherms of niclosamide cocrystals. The single endotherm at a temperature different from the melting points of the pure components is indicative of a homogeneous cocrystal phase. Caffeine (mp 227−228 °C), urea (mp 132−135 °C), PABA (mp 187−189 °C), theophylline (mp 270−274 °C), nicotinamide (mp 128−131 °C), isonicotinamide (mp 157−158 °C).

dx.doi.org/10.1021/cg300784v | *Cryst. Growth Des.* 2012, 12, 4588−4599

Table 3. Melting Point Comparison of Niclosamide Cocrystals

	mp of API (°C)	mp of coformer (°C)	mp of cocrystals (°C), (DSC, T_{Peak})
NCL	229−230		
NCL−CAF		227−228	204−207
NCL−URE		132−135	209−210
NCL−PABA		187−189	186−188
NCL−THPH		270−274	209−210
NCL−THPHS		270−274	83−87, 209−210
NCL−NCT		128−131	215−216
NCL−INA		155−158	227−229

NCL−THPH was stable for 2 weeks but after that started transforming to the hydrate. There is possibility of NCL−THPH hydrate forms after 2−3 weeks in humidity chamber as judged by DSC and TGA (Figure S6). No hydrate was observed for NCL−NCT and NCL−INA cocrystals at 7 weeks in the same conditions (Figure S5). Stability profile of niclosamide cocrystals are summarized in Table 6. NCL−NCT and NCL−INA cocrystals (even though no single crystal XRD is available) are the most stable and did not transform to monohydrate after 7 weeks.

Solubility of Niclosamide Cocrystals. Fast dissolution and high solubility, referred to as bioavailability, are necessary for a solid dosage form to exert its therapeutic effect. Since different crystal forms have different lattice energies and enthalpies, it follows that their solubility will be different. Niclosamide is sparingly soluble in water (13 ± 3 mg/L). Vantonder et al.[5c] carried out dissolution experiments of niclosamide and its monohydrates (H_A and H_B) in 40% i-PrOH−water medium. Solubility of niclosamide increased to 43 mg/L in alcohol−water mixture. Powder dissolution experiments of niclosamide and its cocrystals were carried out on a U.S. Pharmacopeia (USP) approved dissolution tester in the same medium (40% i-PrOH−water) by the rotating paddle method (100 rpm) on powder sieved to 200 μm particle size. Powder dissolution curves for niclosamide cocrystals are shown in Figure 12. An increase in solubility can increase the tendency for phase transformation to hydrate. The cocrystals transformed to hydrate within 1 h of dissolution experiment as indicated by the UV−vis absorption peak at 221 nm[5d] for niclosamide monohydrate. Among the crystalline forms studied, niclosamide−theophylline acetonitrile solvate (NCL−THPHS) exhibited the highest dissolution rate and solubility (223.1 mg/L at 2 h). NCL−THPH cocrystal exhibited comparable dissolution rate to NCL−THPHS for 90 min and the second highest solubility (181.2 mg/L) in powder dissolution experiment at 2 h. NCL−CAF had intermediate solubility (108.4 mg/L) between NCL and NCL−THPHS. The remaining cocrystals, such as NCL−URE, NCL−NCT, and NCL−INA, showed comparatively lower solubility of 67.3, 55.9, and 62.3 mg/L. Surprisingly the solubility of NCL−PABA (28.2 mg/L) was lower than that of the API. The intermolecular N−H···O hydrogen bond distance between the API and PABA is long (1.82 Å), and we surmise that the weak link may result in faster dissociation of cocrystal and hydration of the free API thereby resulting in the observed low solubility of the drug. To summarize, NCL−THPHS and NCL−THPH are 6.3 and 5.1 times more soluble than niclosamide at 2 h. Recently Smith et al.[24] reported quercetin−caffeine (1:1) and quercetin−caffeine MeOH solvate (1:1:1) with 14- and 8-fold increase in solubility of quercetin and 10-fold bioavailability compared to quercetin dihydrate. Generally solvates are not preferred in API formulation because of their instability, phase transformation, and volatile byproduct. Here acetonitrile solvate crystals were not stable at ambient conditions and moreover CH_3CN is a class II solvent[25] with permissible concentration limit of 410 ppm. In comparison, NCL−THPH cocrystal appears to be the best choice in terms of good stability and improved solubility. Most drugs exert their therapeutic effect within 4−6−8 h of oral administration. High coformer solubility confers improved solubility to the drug cocrystal.[3a,c,26] NCT−URE seems to be an exception since the high solubility of urea (1.1 g/mL) did not reflect in the cocrystal (only 2-fold higher). Again theophylline (solubility 8 mg/mL) is the least soluble cofomer but NCL−THPH cocrystal exhibited the second highest solubility. The melting points of cocrystals are lower than that of niclosamide, and there was no simple relation between melting point and solubility. NCL−PABA cocrystal of lowest melting point (186 °C) is the least soluble and NCL−INA has highest melting point (228 °C) and two times more soluble.

Solubility is a thermodynamic quantity and usually taken as the concentration of the solute at 24 or 48 h after mixing in a solvent. The miniaturized shake-flask method[27] was used to determine equilibrium solubility of niclosamide cocrystals. The amount of drug required in this method is more to ensure that undissolved solid phase is in equilibrium with the saturated solution. This method is therefore unsuited for those drug forms that are metastable and undergo phase transformation during the slurry conditions of dissolution. Equilibrium solubility was measured by dissolving the crystalline form (100 mg) in a minimum amount of 40% i-PrOH−water solvent

Table 4. FT-IR Stretching Modes (ν_s, cm^{-1}) of Niclosamide Cocrystals

	O−H stretch	N−H stretch	N−H bend	C=C stretch	C=O stretch	C−O stretch	NO_2 asymm stretch	NO_2 sym stretch
NCL		3242.7, 3199.5	1570.4	1613.5, 1588.9	1652.7	1217.9	1520.9	1348.4, 1329.7
NCL HYD	3577.3, 3490.4	3241.5, 3197.9	1569.7	1613.2, 1604.8	1680.1, 1652.9	1218.1	1517.3	1348.2, 1328.3
NCL−CAF		3256.2	1556.5	1605.1, 1581.5	1705.3, 1674.9	1216.4	1508.1	1340.0, 1323.3
NCL−URE	3491.6, 3438.5	3352.9, 3249.5	1545.0	1605.3	1673.9	1225.3	1512.0	1342.9, 1321.1
NCL−PABA	3461.9	3364.1, 3253.9	1547.8	1606.6	1672.0	1217.7	1504.5	1344.1, 1320.5
NCL−THPH		3260.4, 3160.6	1555.9	1601.4	1697.5, 1674.7	1218.7	1509.0	1343.8, 1323.5
NCL−THPHS		3262.3, 3126.1	1552.3	1604.0	1698.0, 1673.0, 1639.5	1219.0	1508.6	1340.3, 1321.4
NCL−NCT	3409.0	3305.4, 3235.8, 3168.8	1557.5	1607.4, 1582.6	1737.2, 1712.7, 1665.0	1225.0	1518.4	1347.5, 1322.7
NCL−INA	3445.2	3237.3, 3159.6	1560.7	1609.2, 1583.2	1707.4, 1665.0	1220.1	1523.0	1344.5, 1323.8

dx.doi.org/10.1021/cg300784v | Cryst. Growth Des. 2012, 12, 4588−4599

Table 5. FT-Raman Stretching Modes (ν_s, cm^{-1}) of Niclosamide Cocrystals

	C−H stretch	N−H bend	C=C stretch	C=O stretch	C−O stretch	NO_2 asymm stretch	NO_2 sym stretch
NCL	3069.5, 3103.8	1560.9	1587.3	1649.7	1216.5	1509.5	1348.1, 1325.8
NCL HYD	3070.1, 3102.2	1562.1	1588.3	1650.5	1217.7	1509.2	1348.6, 1327.3
NCL−CAF	3081.7	1548.0	1600.3, 1578.9	1707.8, 1676.9	1215.4		1340.0, 1318.8
NCL−URE	3098.2, 3073.0	1543.3	1582.2	1675.3	1222.9		1345.2, 1317.7
NCL−PABA	3075.0	1547.9	1599.0, 1580.8	1663.9	1216.7	1508.0	1340.4, 1322.4
NCL−THPH	3066.8	1535.2	1583.3	1726.3, 1674.5	1215.9	1506.5	1343.9, 1317.8
NCL−THPHS	3126.4, 3067.4	1542.2	1583.4	1675.1	1218.1	1506.2	1342.5, 1316.4
NCL−NCT	3072.7		1585.1	1661.2	1219.1	1519.8	1321.7, 1347.4
NCL−INA	3084.6		1583.2	1665.2	1233.2, 1223.0	1524.3	1343.7, 1323.1

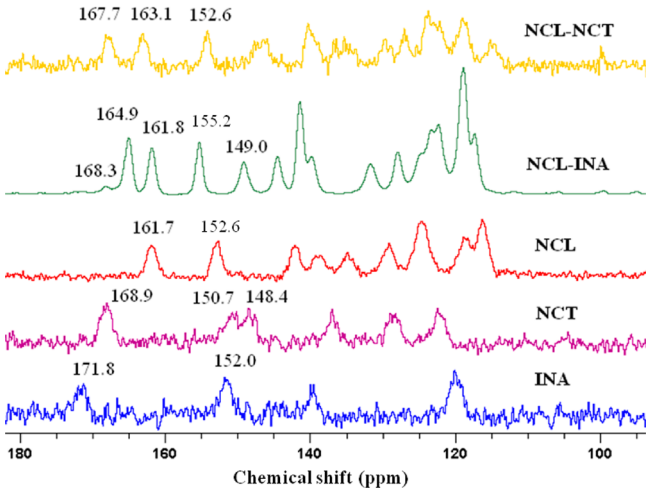

Figure 10. Solid-state ^{13}C NMR spectra of NCL−NCT and NCL−INA cocrystal. The change in carbonyl peak shift indicates a new solid phase.

(5 mL) and stirred for 24 h at 37 °C. Niclosamide showed higher solubility (43 mg/L) in alcohol−water mixture, which is in reality the solubility of niclosamide monohydrate after 24 h of slurry. The dissolved drug concentration at 2 and 24 h of dissolution experiment are listed in Table 7. All crystalline forms converted to niclosamide monohydrate (H_A) after 24 h (as confirmed by IR spectroscopy) and for this reason solubility of all cocrystals is very close.

CONCLUSION

Modification of the physicochemical properties of a crystalline API by introducing a pharmaceutically acceptable compound is a current strategy in drug formulation and dosage optimization. Niclosamide is almost insoluble in water. Pharmaceutical cocrystals of niclosamide are reported with GRAS molecules for the first time. Niclosamide is prone to solvate and hydrate formation and hence there are limitations to the wet-granulation method for cocrystal preparation. Dry solvents are required to prepare niclosamide cocrystals by solvent-assisted grinding. All new crystalline forms were characterized by spectroscopy, thermal analysis, and X-ray diffraction. The hydrogen bonds in niclosamide structure are changed by the presence of coformers containing COOH, CONH, OH, NH functional groups. NCL−THPHS solvate had the fastest dissolution rate (6 times), but it was prone to hydrate formation within 2−3 days under ICH conditions. The permissible concentration limit of class II solvent acetonitrile is 410 ppm. In comparison, NCL−THPH showed the second best dissolution rate (5 times) and moderate stability (2 weeks) toward hydration. All cocrystals exhibited faster dissolution rate and higher stability toward hydration than the reference drug except NCL−PABA. The search for new GRAS coformers with better improvement in solubility and stability continues to be explored.

EXPERIMENTAL SECTION

Niclosamide and other GRAS coformers were purchased from Sigma-Aldrich (Hyderabad, India) and used directly for experiments. All other chemicals were of analytical or chromatographic grade. Melting points were measured on a Fisher-Johns melting point apparatus. Water filtered through a double deionized purification system (AquaDM, Bhanu, Hyderabad, India) was used in all experiments. Single crystals were obtained via slow evaporation of stoichiometric amounts of starting materials in an appropriate solvent after grinding in a mortar-pestle. Cocrystals and hydrate/solvate were characterized by IR, PXRD, DSC, TGA, and single crystal X-ray diffraction (SC-XRD).

Niclosamide, NCL. Niclosamide crystals were obtained from sublimation at 190−200 °C. Good quality rectangular plate crystal appeared after 4−5 h. Single crystals were also obtained by crystallization from AcOH. mp 229−230 °C.

NCL−CAF (1:1) Cocrystal. 100 mg (0.31 mmol) of niclosamide and 59.4 mg (0.31 mmol) of caffeine were ground in mortar-pestle for 15 min after adding 5 drops of dry EtOAc, and then kept for crystallization in 10 mL of EtOAc. Suitable square block crystals appeared at ambient conditions after 3−4 days. mp 204−206 °C.

NCL−URE (1:1) Cocrystal. 100 mg (0.31 mmol) of niclosamide and 18.4 mg (0.31 mmol) of urea were ground in mortar-pestle for 15 min after adding 5 drops of dry EtOAc, and then kept for crystallization in 10 mL of EtOAc. Suitable thick plate crystals were harvested at ambient conditions after 3−4 days. mp 209−210 °C.

NCL−PABA (1:1) Cocrystal. 100 mg (0.31 mmol) of niclosamide and 41.9 mg (0.31 mmol) of PABA were ground in mortar-pestle for 15 min after adding 5 drops of dry EtOAc, and then kept for crystallization in 10 mL of EtOAc. Suitable block crystals were harvested at ambient conditions after 3−4 days. mp 186−188 °C.

NCL−THPH (1:1) Cocrystal. 100 mg (0.31 mmol) of niclosamide and 55.1 mg (0.31 mmol) of theophylline were ground in mortar-pestle for 15 min after adding 5 drops of dry isopropyl acetate, and then kept for crystallization in 10 mL of isopropyl acetate. Suitable block crystals were harvested at ambient conditions after 3−4 days. mp 209−210 °C.

NCL−THPHS (1:1:1) Complex. 100 mg (0.31 mmol) of niclosamide and 55.1 mg (0.31 mmol) of theophylline were ground in mortar-pestle for 15 min after adding 5 drops of dry acetonitrile, and then kept for crystallization in 10 mL of EtOAc−acetonitrile (1:1) mixture. Suitable block crystals were harvested at ambient conditions after 3−4 days. mp 209−210 °C. Desolvation temperature for acetonitrile solvate 83−87 °C.

NCL−NCT (1:1) and NCL−INA (1:1) Cocrystal. 100 mg (0.31 mmol) of niclosamide and 37.4 mg (0.31 mmol) of nicotinamide (or isonicotinamide) were ground in a mortar-pestle for 15 min after adding 5 drops of dry EtOAc. No single crystals were obtained in several solvents attempted. Solution ^1H NMR (DMSO-d_6 solvent) and

dx.doi.org/10.1021/cg300784v | Cryst. Growth Des. 2012, 12, 4588−4599

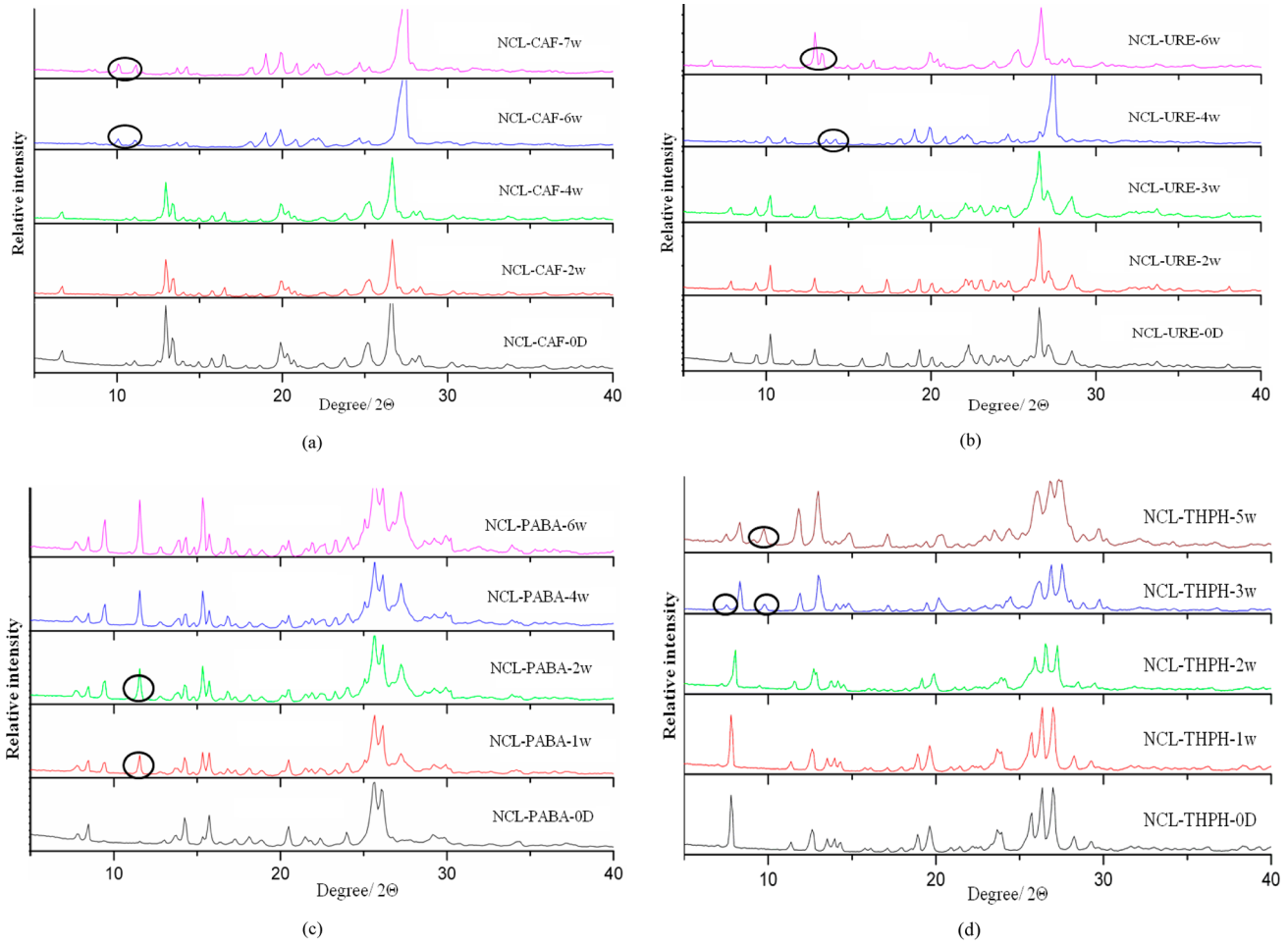

Figure 11. PXRD stack plots of (a) NCL−CAF, (b) NCL−URE, (c) NCL−PABA, and (d) NCL−THPH kept in accelerated ICH conditions of 40 °C and 75% RH. Peaks at 2θ 7.86, 9.47, 10.37, 11.40, 16.83, 19.02° suggest formation of niclosamide hydrate after 1 week.

Table 6. Stability of Niclosamide Cocrystals under ICH Conditions of 40 °C and 75% RH[a]

	1W	2W	3W	4W	5W	6W	7W
NCL	X	X	X	X	X	X	X
NCL−CAF	√	√	√	√	√	X	X
NCL−URE	√	√	√	X	X	X	X
NCL−PABA	√	X	X	X	X	X	X
NCL−THPH	√	√	X	X	X	X	X
NCL−THPHS	X	X	X	X	X	X	X
NCL−NCT	√	√	√	√	√	√	√
NCL−INA	√	√	√	√	√	√	√

[a]W = week, X = hydrate formation started, √ = no hydrate formation.

solid-state ^{13}C NMR suggested that cocrystals stoichiometry is 1:1 of niclosamide and nicotinamide/isonicotinamide. mp NCL−NCT (1:1) 215−216 °C and NCL−INA (1:1) 227−229 °C.

X-ray Crystallography. Single crystal obtained from the crystallization solvent(s) was mounted on the goniometer of Oxford Gemini (Oxford Diffraction, Yarnton, Oxford, UK) or Bruker Smart (Bruker-AXS, Karlsruhe, Germany) equipped with Mo−Kα radiation (λ = 0.71073 Å) source. Data reduction was performed using CrysAlisPro 171.33.55 software.[28] Crystal structures were solved and refined using Olex2−1.0[29] with anisotropic displacement parameters for non-H atoms. Hydrogen atoms were experimentally located through the Fourier difference electron density maps in all crystal structures. All aromatic C−H atoms were geometrically fixed using HFIX command in SHELX-TL program of Bruker-AXS.[30] A check of the final .cif file with PLATON[31] did not show any missed symmetry. X-Seed[32] was used to prepare the figures and packing diagrams. Crystallographic parameters of crystal structures are summarized in Table 1. Hydrogen bond distances in Table 2 are neutron-normalized

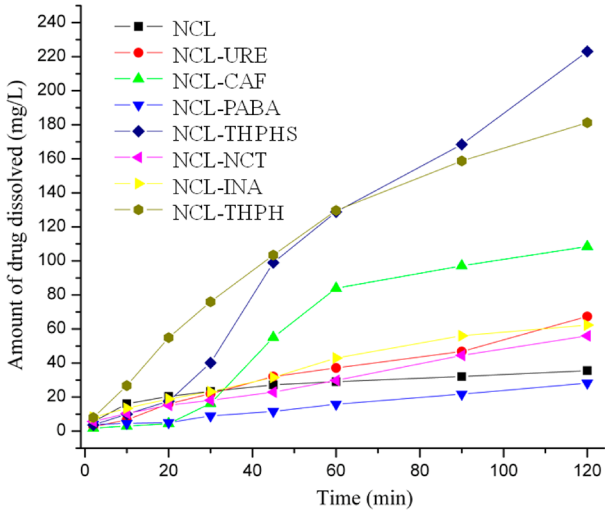

Figure 12. Powder dissolution curve for niclosamide cocrystals in 40% i-PrOH−water. NCL (black), NCL−CAF (green), NCL−URE (red), NCL−PABA (blue), NCL−THPH (dark yellow), NCL−THPHS (navy blue), NCL−NCT (magenta), and NCL−INA (yellow).

dx.doi.org/10.1021/cg300784v | Cryst. Growth Des. 2012, 12, 4588−4599

Table 7. Solubility Profile of Niclosamide Cocrystals

	absorption coefficient (ε, mM^{-1} cm^{-1})	solubility at 37 °C (24 h) in 40% i-PrOH–water (mg L^{-1})	solubility at 37 °C in 40% i-PrOH–water (mg L^{-1}) at 2 h of dissolution[a]
NCL	16.95	42.8	35.53
NCL–CAF	19.18	56.7	108.45 (x3.0)
NCL–URE	13.35	84.3	67.34 (x1.9)
NCL–PABA	19.89	32.8	28.22 (x0.8)
NCL–THPH	13.01	60.4	181.19 (x5.1)
NCL–THPHS	16.02	56.2	223.09 (x6.3)
NCL–NCT	14.72	53.1	55.97 (x1.6)
NCL–INA	15.87	71.9	62.33 (x1.7)

[a]Number in parentheses indicates number of times higher solubility of cocrystal compared to reference niclosamide.

to fix the D–H distance to its accurate neutron value in the X-ray crystal structures (O–H 0.983 Å, N–H 0.82 Å, C–H 1.083 Å). Crystallographic .cif files (CCDC Nos. 892330–\892335) are available at www.ccdc.cam.ac.uk/data_request/cif or as part of Supporting Information.

Powder X-ray Diffraction. Bulk samples were analyzed by PXRD with a Bruker AXS D8 powder diffractometer (Bruker-AXS, Karlsruhe, Germany). Experimental conditions: Cu–Kα radiation (λ = 1.54056 Å); 40 kV; 30 mA; scanning interval 5–50° 2θ at a scan rate of 1°/min; time per step 0.5 s. The experimental PXRD patterns and calculated X-ray lines from crystal structures were compared to confirm purity of the bulk phase using Powder Cell.[33]

Thermal Analysis. DSC and TGA were performed on a Mettler Toledo DSC 822e module and a Mettler Toledo TGA/SDTA 851emodule, respectively. Samples were placed in open alumina pans for TGA and in crimped but vented aluminum sample pans for DSC. A typical sample size is 4–6 mg for DSC and 9–12 mg for TGA. The temperature range was 30–250 at 2 °C/min for DSC and at 10 °C/min for TGA. Samples were purged with a stream of dry N_2 flow at 150 mL/min for DSC and 50 mL/min for TGA.

Vibrational Spectroscopy. A Thermo-Nicolet 6700 FT-IR spectrometer (Waltham, MA, USA) with NXR FT-Raman Module (Nd:YAG laser source, 1064 nm wavelength) was used to record IR and Raman spectra. IR spectra were recorded on samples dispersed in KBr pellets. Raman spectra were recorded on samples contained in standard NMR diameter tubes or on compressed samples contained in a gold-coated sample holder.

Solid-State NMR Spectroscopy. The solid-state ^{13}C NMR spectra were obtained on a Bruker Ultrashield 400 spectrometer (Bruker BioSpin, Karlsruhe, Germany) utilizing a ^{13}C resonant frequency of 100 MHz (magnetic field strength of 9.39 T). Approximately 100 mg of crystalline sample was lightly packed into a zirconium rotor with a Kel-F cap. The cross-polarization, magic angle spinning (CP-MAS) pulse sequence was used for spectral acquisition. Each sample was spun at a frequency of 5.0 ± 0.01 kHz and the magic angle setting calibrated by the KBr method. Each data set was subjected to a 5.0 Hz line broadening factor and subsequently Fourier transformed and phase corrected to produce a frequency domain spectrum. The chemical shifts were referenced to TMS using glycine ($\delta_{glycine}$ = 43.3 ppm) as an external secondary standard.

Dissolution and Solubility Experiments. Powder dissolution rate (PDR) and solubility measurements were carried out on a USP-certified Electrolab TDT-08 L dissolution tester (Electrolab, Mumbai, India). A calibration curve was obtained for all new solid phases (including niclosamide) of absorbance vs concentration UV–vis spectra on a Thermo Scientific Evolution EV300 (Waltham, MA, USA) for known concentration solutions in 40% i-PrOH–water medium. The mixed solvent system was selected because niclosamide has higher solubility in this medium. The slope of the plot from the standard curve gave the molar extinction coefficient (ε) by applying Beer–Lambert's law. Equilibrium solubility was determined in 40% i-PrOH–water medium using the shake-flask method.[27] To determine the equilibrium solubility, 100 mg of each solid material was stirred for 24 h in 5 mL of 40% i-PrOH–water at 37 °C, and the absorbance was measured at 337 nm. The concentration of the saturated solution was calculated at 24 h, which is referred to as the equilibrium solubility of the stable solid form.

For powder dissolution studies of niclosamide and its cocrystals, the starting solids were sieved in ASTM standard mesh sieves to provide samples with particle size of approximately 200 μm and then directly poured into 900 mL of dissolution medium, and the paddle rotation was fixed at 100 rpm. Dissolution experiments were continued up to 2 h at 37 °C. At regular intervals of 5–10 min, 5 mL of the dissolution medium was drawn and replaced by an equal volume of fresh medium to maintain a constant volume. The amount of niclosamide dissolved was calculated from the plot of dissolved niclosamide (mg/L) vs time (min).

■ ASSOCIATED CONTENT

Ⓢ Supporting Information

Additional NMR, IR, PXRD and DSC plots, and crystallographic .cif files are available free of charge via the Internet at http://pubs.acs.org.

■ AUTHOR INFORMATION

Corresponding Author

*E-mail: ashwini.nangia@gmail.com.

Notes

The authors declare no competing financial interest.

■ ACKNOWLEDGMENTS

We thank DST (JC Bose fellowship SR/S2/JCB-06/2009) and CSIR (Pharmaceutical cocrystals 01(2410)/10/EMR-II) for research funding, and DST (IRPHA) and UGC (PURSE grant) for providing instrumentation and infrastructure facilities. P.S. and S.S.K. thank UGC and CSIR for a fellowship.

■ REFERENCES

(1) (a) Lipinski, C. *Am. Pharm. Rev.* **2002**, *5*, 82. (b) Datta, S.; Grant, D. J. W. *Nat. Rev. Drug Discovery* **2004**, *3*, 42. (c) Vippagunta, S. R.; Brittain, H. G.; Grant, D. J. W. *Adv. Drug Delivery Rev.* **2001**, *48*, 3. (d) Yu, L. *Adv. Drug Delivery Rev.* **2001**, *48*, 27. (e) Byrn, S. R.; Pfeiffer, R. R.; Stowell, J. G. *Solid-State Chemistry of Drugs*, 2nd ed.; SSCI, Inc.: West Lafayette, IN, 1999.

(2) (a) Curatolo, W. *Pharm. Sci. Technol. Today* **1998**, *1*, 387. (b) Huang, L. F.; Tong, W. Q. *Adv. Drug Delivery Rev.* **2004**, *56*, 321. (c) Bastin, R. J.; Bowker, M. J.; Slater, B. J. *Org. Process Res. Dev.* **2000**, *4*, 427. (d) Morris, K. R.; Fakes, M. G.; Thakur, A. B.; Newman, A. W.; Singh, A. K.; Venit, J. J.; Spagnuolo, C. J.; Serajuddin, A. T. M. *Int. J. Pharm.* **1994**, *105*, 209.

(3) (a) Remenar, J. F.; Morissette, S. L.; Peterson, M. L.; Moulton, B.; MacPhee, J. M.; Guzmán, H. R.; Almarsson, Ö. *J. Am. Chem. Soc.* **2003**, *125*, 8456. (b) Galcera, J.; Molins, E. *Cryst. Growth Des.* **2009**, *9*, 327. (c) Childs, S. L.; Chyall, L. J.; Dunlap, J. T.; Smolenskaya, V. N.; Stahly, B. C.; Stahly, G. P. *J. Am. Chem. Soc.* **2004**, *126*, 13335. (d) Stanton, M. K.; Tufecic, S.; Morgan, C.; Bak, A. *Cryst. Growth Des.* **2009**, *9*, 344. (e) Trask, A. V.; Motherwell, W. D. S.; Jones, W. *Int. J. Pharm.* **2006**, *320*, 114. (f) Reddy, L. S.; Babu, N. J.; Nangia, A. *Chem. Commun.* **2006**, 499. (g) McNamara, D. P.; Childs, S. L.; Giordano, J.; Iarriccio, A.; Cassidy, J.; Shet, M. S.; Mannion, R.; O'Donnell, E.; Park, A. *Pharm. Res.* **2006**, *23*, 1888. (h) Vishweshwar, P.; McMahon, J. A.; Bis, J. A.; Zaworotko, M. J. *J. Pharm. Sci.* **2006**, *95*, 499. (i) Chow, S. F.; Chen, M.; Shi, L.; Chow, A. H. L.; Sun, C. C. *Pharm. Res.* **2012**, *29*,

1854. (j) Babu, N. J.; Nangia, A. *Cryst. Growth Des.* **2011**, *11*, 2662. (k) Tumanov, N. A.; Myz, S. A.; Shakhtshneider, T. P.; Boldyreva, E. V. *CrystEngComm* **2012**, *14*, 305.
(4) Generally Regarded as Safe: http://www.cfsan.fda.gov/_rdb/opagras.html and http://www.cfsan.fda.gov/~dms/grasguid.html.
(5) (a) Caira, M. R.; Vantonder, E. C.; Villers, M. M. D.; Lötter, A. P. *J. Incl. Phenom. Mol. Recogn. Chem.* **1998**, *31*, 1. (b) Vantonder, E. C.; Mahlatji, M. D.; Malan, S. F.; Liebenberg, W.; Caira, M. R.; Song, M.; Villers, M. M. D. *AAPS PharmSciTech.* **2004**, *5*, 86. (c) Vantonder, E. C.; Maleka, T. S. P.; Liebenberg, W.; Song, M.; Wurster, D. E.; Villers, M. M. D. *Int. J. Pharm.* **2004**, *269*, 417. (d) Villers, M. M. D.; Mahlatji, M. D.; Vantonder, E. C.; Malan, S. F.; Lötter, A. P.; Liebenberg, W. *Drug Dev. Ind. Pharm.* **2004**, *30*, 581. (e) Manek, R. V.; Kolling, W. M. *AAPS PharmSciTech.* **2004**, *5*, 1. (f) Tian, F.; Qu, H.; Louhi-Kultanen, M.; Rantanen, J. *Chem. Eng. Technol.* **2010**, *33*, 833.
(6) Wu, C. -J.; Jan, J. -T.; Chen, C. -M.; Hsieh, H. -P.; Hwang, D. -R.; Liu, H. -W.; Liu, C. -Y.; Huang, H. -W.; Chen, S. -C.; Hong, C. -H.; Lin, R. -K.; Chao, Y. -S.; Hsu, J. T. A. *Antimicrob. Agents Chemother.* **2004**, *48*, 2693.
(7) Lindenberg, M.; Kopp, S.; Dressman, J. B. *Eur. J. Pharm. Biopharm.* **2004**, *58*, 265.
(8) *British Pharmacopeia*; Her Majesty's Stationery Office: London, 1993; p 445.
(9) (a) Van Tonder, E. C. Preparation and Characterization of Niclosamide Crystal Modifications. Ph.D. Thesis, Potchefstroom University for CHE, South Africa, 1996. (b) Maleka, T. S. P. Aqueous adsorption and desorption behavior of niclosamide anhydrate and monohydrates. M.Sc dissertation, 2000
(10) Graebing, P. W.; Chib, J. S.; Hubert, T. D.; Gingerich, W. H. *J. Agric. Food Chem.* **2004**, *52*, 870.
(11) Campeta, A. M.; Chekal, B. P.; Abramov, Y. A.; Meenan, P. A.; Henson, M. J.; Shi, B.; Singer, R. A.; Horspool, K. R. *J. Pharm. Sci.* **2010**, *99*, 3874.
(12) (a) Edwards, H. G. M.; Lawson, E.; Matas, M. D.; Shields, L.; York, P. *J. Chem. Soc., Perkin Trans. 2* **1997**, 1985. (b) Trask, A. V.; Motherwell, W. D. S.; Jones, W. *Cryst. Growth Des.* **2005**, *5*, 1013. (c) Pienaar, E. W.; Caira, M. R.; Lötter, A. P. *J. Crystallogr. Spectr. Res.* **1993**, *23*, 739.
(13) (a) Ding, K; Pei, D.; Zhou, J. CN101775032 (A), 2010. (b) Zhang, D. J. CN101006778 (A), 2007.
(14) (a) Portell, A.; Barbas, R.; Font-Bardia, M.; Dalmases, P.; Prohens, R.; Puigjaner, C. *CrystEngComm* **2009**, *11*, 791. (b) Thakuria, R.; Nangia, A. *CrystEngComm* **2011**, *13*, 1759. (c) Banerjee, R.; Bhatt, P. M.; Ravindra, N. V.; Desiraju, G. R. *Cryst. Growth Des.* **2005**, *5*, 2299.
(15) (a) Sarma, B.; Roy, S.; Nangia, A. *Chem. Commun.* **2006**, 4918. (b) Sarma, B.; Sanphui, P.; Nangia, A. *Cryst. Growth Des.* **2010**, *10*, 2388.
(16) (a) Shan, N.; Toda, F.; Jones, W. *Chem. Commun.* **2002**, 2372. (b) Delori, A.; Friščić, T.; Jones, W. *CrystEngComm* **2012**, *14*, 2350. (c) Sanphui, P.; Bolla, G.; Nangia, A. *Cryst. Growth Des.* **2012**, *12*, 2023.
(17) (a) Etter, M. C.; Macdonald, J. C. *Acta Crystallogr.* **1990**, *B46*, 256. (b) Bernstein, J.; Davis, R. E.; Shimoni, L.; Chang, N. -L. *Angew. Chem., Int. Ed. Engl.* **1995**, *34*, 1555. (c) Grell, J.; Bernstein, J.; Tinhofer, G. *Acta Crystallogr.* **1999**, *B55*, 1030.
(18) (a) Mullen, D.; Hellner., V. *Acta Crystallogr.* **1978**, *B34*, 1624. (b) Hollingsworth, M. D.; Brown, M. E.; Santersiero, B. S.; Huffman, J. C.; Goss, C. R. *Chem. Mater.* **1994**, *6*, 1227.
(19) (a) Karki, S.; Friščić, T.; Fábián, L.; Jones, W. *CrystEngComm* **2010**, *12*, 4038. (b) Thakuria, R.; Nangia, A. *CrystEngComm* **2011**, *13*, 1759.
(20) (a) Stuart, B. H. *Infrared Spectroscopy: Fundamentals and Applications*; John-Wiley: UK, 2004. (b) McCreery, R. L. *Raman Spectroscopy for Chemical Analysis*, John-Wiley: UK, 2000. (c) Smith, E. Dent, G. *Modern Raman Spectroscopy – A Practical Approach*, John-Wiley: UK, 2005. (d) Moffat, M. A.; Jackson, J. V.; Moss, M. S.; Widdop, B., Eds. *Clarke's Isolation and Identification of Drugs in Pharmaceuticals, Body Fluids, and Post Mortem Materials*, 2nd ed.; London, UK: Pharmaceutical Press, 1986.
(21) (a) Reutzel-Edens, S. M.; Bush, J. K.; Magee, P. A.; Stephenson, G. A.; Byrn, S. R. *Cryst. Growth Des.* **2003**, *3*, 897. (b) Li, Z. J.; Abramov, Y.; Bordner, J.; Leonard, J.; Medek, A.; Trask, A. V. *J. Am. Chem. Soc.* **2006**, *128*, 8199. (c) Vogt, F. G.; Clawson, J. S.; Strohmeier, M.; Edwards, A. J.; Pham, T. N.; Watson, S. A. *Cryst. Growth Des.* **2009**, *9*, 921.
(22) (a) Basavoju, S.; Bostroem, D.; Velaga, S. P. *Pharm. Res.* **2008**, *25*, 530. (b) Tao, Q.; Chen, J.-M.; Ma, L.; Lu, T.-B. *Cryst. Growth Des.* **2012**, *12*, 3144.
(23) (a) Stability testing of active pharmaceutical ingredients and finished pharmaceutical products. World Health Organization WHO Technical Report Series, Annex 2, No. 953, 2009. (b) Vangala, V. R.; Chowa, P. S.; Tan, R. B. H. *CrystEngComm* **2011**, *13*, 759.
(24) Smith, A. J.; Kavuru, P.; Wojtas, L.; Zaworotko, M. J.; Shytle, R. D. *Mol. Pharmaceutics* **2011**, *8*, 1816.
(25) http://www.ema.europa.eu/docs/en_GB/document_library/Scientific_guideline/2009/09/WC500002674.pdf.
(26) (a) Nehm, S. J.; Rodrıguez-Spong, B.; Rodrıguez-Hornedo, N. *Cryst. Growth Des.* **2006**, *6*, 592. (b) Good, D. J.; Rodrıguez-Hornedo, N. *Cryst. Growth Des.* **2009**, *9*, 2252.
(27) Glomme, A.; Marz, J.; Dressman, J. B. *J. Pharm. Sci.* **2005**, *94*, 1.
(28) *CrysAlis CCD and CrysAlis RED*, Ver. 1.171.33.55; Oxford Diffraction Ltd, Yarnton, Oxfordshire, UK, 2008.
(29) Dolomanov, O. V.; Bourhis, L. J.; Gildea, R. J.; Howard, J. A. K.; Puschmann, H. OLEX2: A Complete Structure Solution, Refinement and Analysis Program. *J. Appl. Crystallogr.* **2009**, *42*, 339.
(30) *SMART, Ver. 5.625 and SHELX-TL*, Ver. 6.12; Bruker-AXS Inc., Madison, Wisconsin, USA, 2000.
(31) Spek, A. L. *PLATON, A Multipurpose Crystallographic Tool*; Utrecht University, Utrecht, Netherlands, 2002. Spek, A. L. *J. Appl. Crystallogr.* **2003**, *36*, 7–13.
(32) *X-Seed, Graphical Interface to SHELX-97 and POV-Ray, Program for Better Quality of Crystallographic Figures*; Barbour, L. J. University of Missouri-Columbia: Missouri, USA, 1999.
(33) Kraus, N.; Nolze, G. *Powder Cell, Ver. 2.3, A Program For Structure Visualization, Powder Pattern Calculation and Profile Fitting*; Federal Institute for Materials Research and Testing: Berlin, Germany, 2000.